

TT-GaussOcc: Test-Time Compute for Self-Supervised Occupancy Prediction via Spatio-Temporal Gaussian Splatting

Fengyi Zhang¹ Huitong Yang¹ Zheng Zhang² Zi Huang¹ Yadan Luo¹

¹The University of Queensland, Australia ²Harbin Institute of Technology, China

{fengyi.zhang, huitong.yang}@uq.edu.au, darrenzz219@gmail.com,

huang@itee.uq.edu.au, y.luo@uq.edu.au

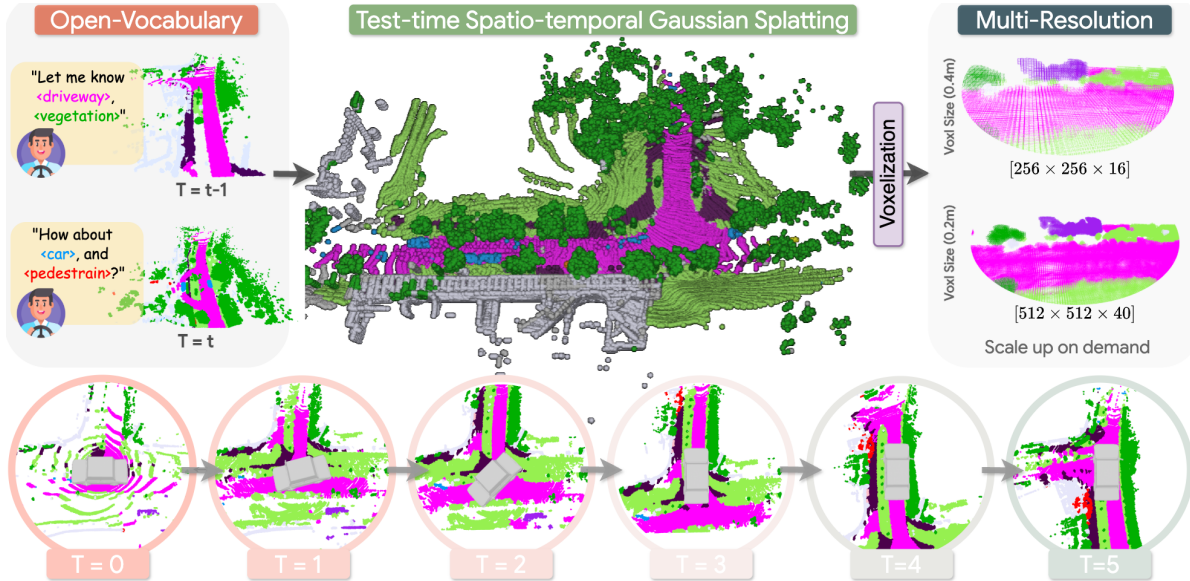


Figure 1. **Overview of TT-GaussOcc for self-supervised occupancy prediction.** Our method incrementally optimizes time-aware 3D Gaussians constructed directly from raw sensor streams, enabling temporally consistent, open-vocabulary occupancy predictions and flexible voxelization at user-defined resolutions. By progressively maintaining static scene Gaussians and updating dynamic objects across time, TT-GaussOcc achieves fine-grained geometry prediction without costly offline training.

Abstract

Self-supervised 3D occupancy prediction offers a promising solution for understanding complex driving scenes without requiring costly 3D annotations. However, training dense voxel decoders to capture fine-grained geometry and semantics can demand hundreds of GPU hours, and such models often fail to adapt to varying voxel resolutions or new classes without extensive retraining. To overcome these limitations, we propose a practical and flexible test-time occupancy prediction framework termed TT-GaussOcc. Our approach incrementally optimizes time-aware 3D Gaussians instantiated from raw sensor streams at runtime, enabling voxelization at arbitrary user-specified resolution. Specifically, TT-GaussOcc operates in a “lift-move-voxel” symphony: we first “lift” surrounding-view semantics obtained from 2D vision foundation models (VLMs) to instan-

tiate Gaussians at non-empty 3D space; Next, we “move” dynamic Gaussians from previous frames along estimated Gaussian scene flow to complete appearance and eliminate trailing artifacts of fast-moving objects, while accumulating static Gaussians to enforce temporal consistency; Finally, we mitigate inherent noises in semantic predictions and scene flow vectors by periodically smoothing neighboring Gaussians during optimization, using proposed trilateral RBF kernels that jointly consider color, semantic, and spatial affinities. The historical static and current dynamic Gaussians are then combined and voxelized to generate occupancy prediction. Extensive experiments on Occ3D and nuCraft with varying voxel resolutions demonstrate that TT-GaussOcc surpasses self-supervised baselines by 46% on mIoU without any offline training, and supports finer voxel resolutions at 2.6 FPS inference speed.

1. Introduction

Occupancy prediction seeks to accurately identify regions within an environment that are occupied by objects of particular classes and those that remain free. Such capability is crucial for enabling collision-free trajectory planning and reliable navigation in autonomous driving systems [36, 41] and embodied agents [14, 30, 37].

Existing occupancy prediction approaches [3, 9, 11, 23, 28, 35, 44] primarily rely on *supervised* learning, which typically requires dense 3D annotations obtained through labor-intensive manual labeling of dynamic driving scenes spanning up to 80 meters per frame. To mitigate this cost, recent studies have resorted to *self-supervised* alternatives [2, 7, 8, 10, 13, 31, 42, 45]. These methods leverage 2D predictions from vision foundation models (VLMs) to train a 3D *occupancy network*, enforcing image reprojection consistency through volume rendering [10, 31, 42] or differentiable rasterization [7]. While effective, these methods still incur substantial computational overhead. For instance, training an occupancy network on Occ3D-nuScenes [28] at a voxel resolution of 0.4m requires approximately 96 hours on eight V100 GPUs [31]. Furthermore, achieving finer resolution (*e.g.*, 0.2m on nuCraft [49]) or adapting to new object classes may necessitate retraining, with computational costs growing *cubically* as resolution increases.

Motivated by these practical limitations, in this work, we investigate a core question: *Is training an occupancy prediction network even necessary?* To this end, we explore a test-time occupancy estimation method termed **TT-GaussOcc**, which progressively optimizes and voxelizes time-aware 3D Gaussians. Our approach eliminates the need for costly pretraining and allows dynamic adaptation to user-specified object classes and voxel resolutions at any given time step. Unlike previous NeRF- [39, 40] and 3DGS-based [6, 48] reconstruction methods that require offline *per-scene* modeling assisted by external priors (*e.g.*, HD maps or bounding boxes), TT-GaussOcc generates occupancy representations in an online fashion, relying solely on raw sensor input streams to instantiate Gaussians capturing object geometry in unbounded outdoor scenes.

Specifically, as depicted in Fig. 2, our approach follows a “*lift-move-voxel*” symphony: (1) At each test time step, we first “*lift*” semantic information into Time-aware Gaussian using surrounding-view segmentation masks from VLMs; (2) Next, we “*move*” the dynamic Gaussians from the previous frame along estimated Gaussian scene flow with iterative closed point (ICP) algorithm. This motion compensates for partial object visibility and prevents trailing artifacts, while static Gaussians are progressively accumulated within a historical queue to maintain long-term temporal coherence. (3) Finally, to minimize inherent noise from 2D semantic predictions and scene flow vectors, we introduce a trilateral radial basis function (TRBF) kernel to period-

ically smooth and optimize Gaussian parameters. The refined static and dynamic Gaussians are subsequently “*voxelized*” onto discrete grids of user-defined resolution.

Extensive experiments on the Occ3D-nuScenes [28] and the recently released nuCraft [49] datasets demonstrate that our TT-GaussOcc improves mIoU by 46% over existing self-supervised counterparts without requiring pretraining. Remarkably, its performance even approaches sparsely supervised occupancy baselines. Under higher-resolution settings, TT-GaussOcc can efficiently generate 10 million voxel predictions per frame at approximately 2.6 FPS, significantly outperforming the state-of-the-art SelfOcc [10] (0.9 FPS), while also reducing VRAM usage by 56%. Qualitative analysis further highlights the superiority of the proposed method in temporal consistency and open-vocabulary generalization.

2. Related Work

2.1. Self-Supervised Occupancy Prediction

Fully supervised occupancy methods predict voxel-level semantics using dense voxel grids [9, 17, 34], depth priors [12, 18], or sparse representations [11, 21, 27]. Despite their effectiveness, these approaches rely heavily on costly large-scale 3D annotations. To mitigate this, recent methods explore self-supervised occupancy learning. SelfOcc [10] leverages signed distance fields (SDF) and multi-view stereo embeddings to achieve temporally consistent occupancy from videos. OccNeRF [42] utilizes photometric consistency and 2D foundation model supervision for semantic occupancy estimation in unbounded scenes. In open-world scenarios, POP3D [29] jointly trains class-agnostic occupancy grids and open-vocabulary semantics using unlabeled paired LiDAR and images, but suffers from sparsity and semantic ambiguity due to low-resolution CLIP [24] features. VEON [45] addresses depth ambiguities via enhanced depth models (MiDaS [25], ZoeDepth [1]) and proposes high-resolution CLIP embeddings, yet still generates sparse semantic attributes that limit fine-grained 3D structures. GaussianOcc [7] uses Gaussian Splatting [15] for cross-view optimization without pose annotations, while GaussianTR [13] aligns rendered Gaussian features with pre-trained foundation models, enabling open-vocabulary occupancy prediction without explicit annotations. Despite these advances, existing methods either rely on extensive offline training or struggle with open-vocabulary settings and fixed resolutions. In contrast, our approach overcomes these limitations by enabling occupancy prediction through temporally coherent, training-free Gaussian optimization at test time.

2.2. 3D Reconstruction of Driving Scenes

Recent advances in dynamic scene modeling have achieved impressive photorealism and multi-view consistency. Om-

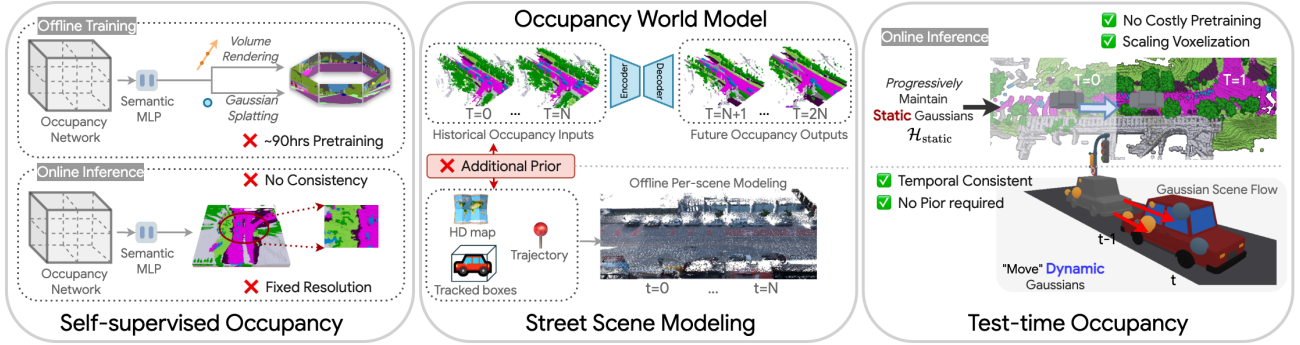


Figure 2. **Overview of different occupancy prediction and scene reconstruction paradigms.** *Left:* Self-supervised occupancy methods require extensive offline training and provide occupancy predictions at a fixed resolution without temporal consistency. *Middle:* Existing street scene modeling or world models utilize additional priors and annotations or historical occupancy to perform *per-scene* reconstruction. *Right:* The proposed TT-GaussOcc dynamically predicts temporally consistent occupancy at test-time by progressively optimizing time-aware static and dynamic 3D Gaussians and enabling scalable voxelization, without costly pretraining or external priors.

niRe [6] performs real-time 3D reconstruction and simulation by building local canonical spaces for dynamic urban actors. Street Gaussians [38] separates moving vehicles from static backgrounds, enabling efficient and high-quality rendering. DrivingGaussian [48] incrementally reconstructs static scenes and dynamically integrates moving objects via Gaussian graphs for interactive editing. HUGS [47] jointly optimizes geometry, appearance, semantics, and motion to achieve real-time view synthesis and 3D semantic reconstruction without explicit bounding box annotations. Autoregressive world modeling methods [32, 46] predict future occupancy using previously estimated 3D occupancies, facilitating temporal reasoning in dynamic environments. As illustrated in Fig. 2, Our test-time approach fundamentally *differs* from these methods by eliminating dependencies on external priors and annotations (e.g., HD maps and GT bounding boxes). Instead, we focus solely on raw sensor inputs, optimizing Gaussian representations independently at each frame to directly infer the accurate geometry of static and dynamic instances, rather than reconstructing photorealistic scenes or predicting future occupancy.

3. Proposed Approach

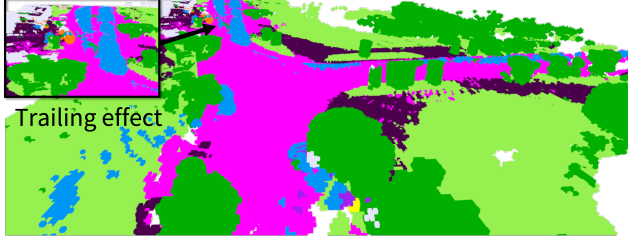
Task Formulation. At each time step t , the objective of occupancy estimation is to infer the voxelized geometry and semantic labels of the current scene directly from raw sensor inputs. Formally, we define the voxel grid as $\mathbf{O}^{(t)} \in \mathbb{C}^{\frac{X}{\delta} \times \frac{Y}{\delta} \times \frac{Z}{\delta}}$, where X, Y, Z defines the spatial dimensions of the region of interest, and δ is the voxel resolution (e.g., 0.2m). The input modality may include a LiDAR point cloud $\mathcal{P}^{(t)} = \{\mathbf{p}_i^{(t)} \in \mathbb{R}^3\}_{i=1}^{N_t}$ and M surrounding-view camera images $\mathcal{I}^{(t)} = \{\mathbf{I}_m^{(t)} \in \mathbb{R}^{3 \times H \times W}\}_{m=1}^M$. Each voxel in $\mathbf{O}^{(t)}$ is assigned a semantic label from the set $\mathbb{C} = \{0, 1, \dots, C\}$, where 0 indicates an empty cell and labels 1 to C corresponds to distinct occupied categories.

Overview of TT-GaussOcc. Rather than training a dense voxel decoder offline, our approach follows “*lift-move-voxel*” *symphony*: ① *Lift*: we first lift surrounding-view semantics obtained from 2D VLMs to instantiate time-aware Gaussians at non-empty 3D space (Sec. 3.1). This step transforms sparse 2D semantic information into meaningful 3D representations without relying on costly dense annotations or pre-trained voxel networks. ② *Move*: Next, we *move* previously instantiated dynamic Gaussians to the current frame via a self-supervised Gaussian scene flow module integrated with iterative closest point (ICP) algorithm. This mechanism effectively compensates for partial visibility in single-frame observations, mitigating trailing artifacts in fast-moving objects, while simultaneously aggregating static Gaussians into a historical queue $\mathcal{H}_{\text{static}}$ to maintain temporal consistency (Sec. 3.2). ③ *Voxel*: Finally, to minimize inherent noise in both the 2D semantic predictions and the 3D flow estimations, we periodically smooth neighboring Gaussians using proposed trilateral radial basis function (TRBF) kernels that consider semantic, color, and spatial affinities. The optimized Gaussians are then splatted back onto the image plane via differentiable rasterization for optimization, and can be adaptively voxelized at arbitrary user-defined resolutions (Sec. 3.3).

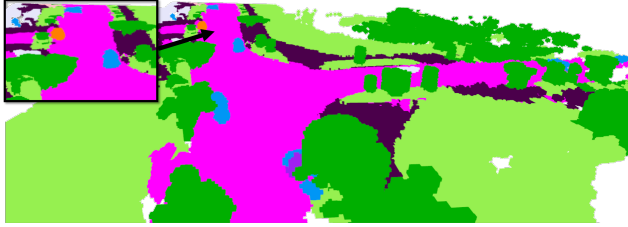
3.1. Lift Semantics of Time-aware Gaussian

For each time step, a set of time-aware Gaussian blobs $\mathcal{G}^{(t)} = \{\mathbf{G}_i^{(t)}\}_{i=1}^{K_t}$ are instantiated to represent scene. Each Gaussian is parameterized by its mean position $\boldsymbol{\mu}_i \in \mathbb{R}^3$, opacity $\alpha_i \in (0, 1)$, color $\mathbf{c}_i \in \mathbb{R}^3$, semantic probability $\mathbf{m}_i \in \mathbb{R}^C$ and the time step t . The spatial density of a 3D Gaussian is given by:

$$\mathbf{G}_i^{(t)}(\mathbf{x}) = \exp\left(-\frac{1}{2}(\mathbf{x} - \boldsymbol{\mu}_i)^\top \boldsymbol{\Sigma}_i^{-1}(\mathbf{x} - \boldsymbol{\mu}_i)\right), \quad (1)$$



(a) Per-frame Gaussian Splatting w/o Flow



(b) Our TT-GaussOcc

Figure 3. (a) Directly optimizing Gaussians per frame can exhibit significant trailing artifacts and distort geometry. (b) Our TT-GaussOcc uses Gaussian scene flow for temporal coherence, effectively reducing trailing and improving occupancy accuracy.

where covariance matrix $\Sigma_i = R(\mathbf{q}_i) \text{diag}(s_i^2) R(\mathbf{q}_i)^\top$ is factorized by the orientation quaternion $\mathbf{q}_i \in \mathbb{R}^4$ and the scale vector $\mathbf{s}_i \in \mathbb{R}_+^3$. To project each Gaussian on the 2D plane, we apply perspective transformation $\text{Proj}(\mathbf{x}; \mathbf{K}, \mathbf{E})$ with the intrinsic matrix $\mathbf{K} \in \mathbb{R}^{3 \times 3}$ and extrinsic matrix $\mathbf{E} \in \mathbb{R}^{3 \times 4}$. The projected mean and covariance are:

$$\boldsymbol{\mu}_i^{2D} = \text{Proj}(\boldsymbol{\mu}_i)_{1:2}, \quad \Sigma_i^{2D} = \mathbf{J}_{\text{Proj}}(\boldsymbol{\mu}_i) \Sigma_i \mathbf{J}_{\text{Proj}}(\boldsymbol{\mu}_i)_{1:2,1:2}^\top,$$

where \mathbf{J}_{Proj} denotes the Jacobian matrix. The color of pixel $\mathbf{u} \in \mathbb{R}^2$ is then blended via alpha compositing,

$$\hat{\mathbf{I}}^{(t)}(\mathbf{u}) = \sum_{i \in \mathcal{N}} \mathbf{c}_i G_i^{2D}(\mathbf{u}) \prod_{j=1}^{i-1} (1 - G_j^{2D}(\mathbf{u})), \quad (2)$$

where $G_i^{2D}(\mathbf{u}) = \alpha_i \exp(-\frac{1}{2}(\mathbf{u} - \boldsymbol{\mu}_i^{2D})^\top (\Sigma_i^{2D})^{-1} (\mathbf{u} - \boldsymbol{\mu}_i^{2D}))$. To incorporate semantic information, we lift 2D semantic labels from M views into 3D Gaussians:

$$\mathbf{m}_i = \frac{1}{M} \sum_{m=1}^M \mathbb{I}_m(\boldsymbol{\mu}_i) \mathcal{M}(\text{Proj}(\boldsymbol{\mu}_i; \mathbf{K}, \mathbf{E})), \quad (3)$$

where $\mathbb{I}_m(\boldsymbol{\mu}_i)$ denoting visibility in the m -th view. The semantic map $\mathcal{M}(\mathbf{u})$ is obtained by querying a foundation VLM *e.g.*, OpenSeeD [43] with the user-specified set of classes \mathcal{C} . Unlike existing self-supervised occupancy counterparts [10], our approach does not rely on a network to decode voxel semantics, thereby supporting *open-vocabulary settings* where target classes can be altered at any time step (See Sec. 4.2).

Voxelization-oriented Initialization. To accelerate Gaussian optimization and subsequent voxelization, we simplify

the standard 3DGS initialization [15]. To maintain computational efficiency, we prune redundant Gaussians within the same voxel cell (size δ) while merging their semantic vectors, ensuring the total number of Gaussians satisfies $K_t \ll N_t$. Additionally, we initialize the scale parameters with δ and constrain them using a sigmoid activation rather than an exponential function to prevent excessive growth.

3.2. Move Dynamics from Gaussian Scene Flow

Reconstructing a driving scene faithfully can be challenging due to fast-moving objects (*e.g.*, vehicles, pedestrians) that are often only partially observed. Without prior knowledge such as complete trajectories or bounding box annotations of moving instances used in [31, 48], optimizing 3D Gaussians online can often result in severe *trailing artifacts* (see Fig. 3). To address this, we propagate the Gaussians from previous time steps by using a learning-free *Gaussian scene flow* estimation, which allows us to relocate and adapt dynamic Gaussians accordingly. Let $\boldsymbol{\mu}^{(t-1)} \in \mathcal{G}^{(t-1)}$ and $\boldsymbol{\mu}^{(t)} \in \mathcal{G}^{(t)}$ be the Gaussian centers at time steps $t-1$ and t in the world coordinate system, respectively. To reduce inliers, ground Gaussians are removed using Patchwork++ [16], and the remaining Gaussians are clustered via CUDA-implemented HDBSCAN [5, 26] for instance association. Given a cluster of object Gaussians at the previous time step $\mathcal{C}^{(t-1)} \subset \boldsymbol{\mu}^{(t-1)}$ and the corresponding cluster at the current step $\mathcal{C}^{(t)} \subset \boldsymbol{\mu}^{(t)}$, we estimate the optimal rigid transformation $\mathbf{T}_C = [\mathbf{R}_C, \mathbf{t}_C]$ via an iterative closest point (ICP)-Flow algorithm [20], which minimizes,

$$\min_{\mathbf{R}_C, \mathbf{t}_C} \sum_{\mathbf{x} \in \mathcal{C}^{(t-1)}} \|\mathbf{R}_C \mathbf{x} + \mathbf{t}_C - \text{NN}(\mathbf{R}_C \mathbf{x} + \mathbf{t}_C, \mathcal{C}^{(t)})\|, \quad (4)$$

where $\text{NN}(\cdot, \mathcal{C}^{(t)})$ returns the nearest neighbor points in $\mathcal{C}^{(t)}$. The estimated Gaussian scene flow for each point $\mathbf{x} \in \boldsymbol{\mu}^{(t-1)}$ is given by:

$$\mathbf{f}_{t-1 \rightarrow t}(\mathbf{x}) = \mathbf{R}_C \mathbf{x} + \mathbf{t}_C - \mathbf{x}. \quad (5)$$

To preserve dynamic objects, their Gaussians are propagated to the current frame:

$$\mathcal{G}^{(t)} \leftarrow \mathcal{G}^{(t)} \cup \mathcal{G}^{(t-1 \rightarrow t)}[\boldsymbol{\mu}^{(t-1)} + \mathbf{f}_{t-1 \rightarrow t}(\boldsymbol{\mu}^{(t-1)}), :] \quad (6)$$

This approach reconstructs the full spatial extent and density of moving objects, leading to more accurate geometry estimations. For *static* Gaussians, where the flow magnitude remains below a small threshold τ , we insert them into a scene Gaussian queue to maintain temporal consistency for subsequent voxelization:

$$\mathcal{H}_{\text{static}} \leftarrow \mathcal{H}_{\text{static}} \cup \{\mathbf{G}_i^{t-1} \mid \|\mathbf{f}_{t-1 \rightarrow t}(\boldsymbol{\mu}_i^{(t-1)})\| < \tau\}. \quad (7)$$

3.3. Spatiotemporal Smoothing and Voxelization

To mitigate the inherent noise and errors in lifted 2D semantic labels (Eq. (3)) and estimated flow vectors (Eq. (4)), we

introduce a Trilateral Radial Basis Function (TRBF) kernel for periodic smoothing and denoising, improving the spatial and temporal coherence of occupancy predictions by leveraging spatial, radiometric, and semantic affinities among Gaussians.

Trilateral RBF Kernel. Unlike uniform aggregation, our TRBF kernel leverages the covariance structure of 3D Gaussians to guide anisotropic information propagation, preserving local object structures and semantic boundaries. Formally, for each $\mathbf{m}_i \in \mathbf{G}_i^{(t)}$, the kernel smoothing is defined as a deformable convolutional over its nearest neighbors:

$$\mathbf{m}_i \leftarrow \frac{1}{Z(i)} \sum_{j \in \text{NN}(i)} \mathbf{m}_j \cdot \mathcal{K}(i, j), \quad (8)$$

where $\text{NN}(\cdot)$ identifies K nearest Gaussians using a kd-tree for efficient search and $Z(i)$ is a normalization factor $Z(i) = \sum_{j \in \text{NN}(i)} \mathcal{K}(i, j)$. By the Schur Product Theorem, the trilateral kernel decomposes element-wise into spatial, radiometric, and semantic components:

$$\mathcal{K}(i, j) = \mathcal{K}_{\text{spatial}}(i, j) \cdot \mathcal{K}_{\text{radio}}(i, j) \cdot \mathcal{K}_{\text{sem}}(i, j). \quad (9)$$

Specially, each term is defined as,

$$\mathcal{K}_{\text{spatial}} = \exp\left(-\frac{(\boldsymbol{\mu}_i - \boldsymbol{\mu}_j)^\top \boldsymbol{\Sigma}_{ij}^{-1} (\boldsymbol{\mu}_i - \boldsymbol{\mu}_j)}{2\sigma_\mu^2}\right),$$

$$\mathcal{K}_{\text{radio}} = \exp\left(-\frac{\|\mathbf{c}_i - \mathbf{c}_j\|^2}{2\sigma_c^2}\right), \mathcal{K}_{\text{sem}} = \exp\left(-\frac{D_{\text{KL}}(\mathbf{m}_i \parallel \mathbf{m}_j)}{2\sigma_s^2}\right),$$

where $\boldsymbol{\Sigma}_{ij} = (\boldsymbol{\Sigma}_i^{-1} + \boldsymbol{\Sigma}_j^{-1})^{-1}$ is the fused covariance matrix, capturing directional uncertainty and structural alignment. From a signal processing perspective, the trilateral smoothing behaves as a non-stationary low-pass filter with locally adaptive cutoff frequencies. The spatial kernel $\mathcal{K}_{\text{spatial}}$ suppresses high-frequency *geometric* noise while preserving large-scale structures, the radiometric kernel $\mathcal{K}_{\text{radio}}$ attenuates high-frequency variations in appearance space, preventing artifacts due to local *illumination* differences, and the semantic kernel \mathcal{K}_{sem} operates in probability space, enforcing consistency while avoiding over-smoothing across *semantic* boundaries.

Gaussian Optimization. Our model refines the Gaussian parameters at test time by minimizing a loss that enforces color and depth consistency; Notably, our optimization focuses on geometry rather than scene fidelity, with sky regions intentionally masked out following [48]. The loss function for each test frame t combines

$$\mathcal{L} = \sum_{\mathbf{u} \in \mathbf{I}_m^{(t)}} |\hat{\mathbf{I}}_m^{(t)}(\mathbf{u}) - \mathbf{I}_m^{(t)}(\mathbf{u})| + \lambda \sum_{\mathbf{v} \in \mathbf{P}_{2D,m}^{(t)}} |\hat{\mathbf{D}}^{(t)}(\mathbf{v}) - \mathbf{D}^{(t)}(\mathbf{v})|,$$

where the coefficient λ balances the photometric consistency and depth consistency loss. $\mathbf{P}_{2D,m}^{(t)}$ denotes the 2D projection of LiDAR points onto the m -th view.

Gaussian Voxelization. For efficient occupancy estimation, we voxelize the optimized Gaussians alongside static Gaussians with sufficiently high opacity: $\mathbf{V}^{(t)} = \mathcal{G}^{(t)} \cup \mathcal{H}_{\text{static}}$. This set is quantized into a discrete grid $\Omega = [\frac{X}{\delta} \times \frac{Y}{\delta} \times \frac{Z}{\delta}]$, where each Gaussian’s contribution on a voxel is weighted based on its spatial proximity. Formally, the occupancy probability of a voxel $v \in \Omega$ is given by,

$$\mathbb{P}(\mathbf{O}_v^{(t)}) = \frac{1}{Z_v} \sum_{\mathbf{G}_i^{(t)} \in \mathbf{V}^{(t)}} (\mathbf{m}_i \cdot \mathcal{K}_{\text{spatial}}(i, v)), \quad (10)$$

$$\mathcal{K}_{\text{spatial}}(i, v) = \exp\left(-\frac{(\boldsymbol{\mu}_i - \mathbf{x}_v)^\top \boldsymbol{\Sigma}_i^{-1} (\boldsymbol{\mu}_i - \mathbf{x}_v)}{2\sigma_\mu^2}\right)$$

where Z_v is the normalizing factor. This voxelization strategy allows flexible scaling to varying voxel resolutions during test-time, balancing efficiency and precision.

4. Experiments

4.1. Experiment Setup

Experiments were conducted on the widely used nuScenes [4] benchmark using 3D occupancy GT from **Occ3D-nuScenes** [28] and **nuCraft** [49]. The nuScenes dataset consists of 600 training scenes and 150 validation ones. Existing supervised and self-supervised methods typically require extensive offline training on the training split. In contrast, TT-GaussOcc requires no pretraining and is directly evaluated on the validation split. In particular, **Occ3D-nuScenes** [28] provides voxelized occupancy annotations at $0.4m$ resolution, covering a spatial range of $[-40m, 40m]$ along the X and Y axes and $[-1m, 5.4m]$ along the Z axis. **nuCraft** [49] offers more finer-grained annotations with a resolution of $0.2m$, covering $[-51.2m, 51.2m]$ in the X and Y directions and $[-5m, 3m]$ in the Z direction. Compared to offline-trained models, which require a predefined class set before training, our test-time approach generalizes dynamically to arbitrary object classes without retraining. For a fair comparison, we follow standard evaluation protocols, reporting results on 16 predefined classes, while open-vocabulary generalization is explored separately in Sec. 4.2.

We evaluate semantic occupancy prediction using mean Intersection over Union (mIoU), computed as the average IoU across all classes. Following prior works [7, 13, 42], we exclude the “noise” and “other flat” categories, as these do not correspond to valid prompts in open-vocabulary segmentation. Additionally, we report inference speed and memory consumption (VRAM) to provide a comprehensive comparison with SelfOcc [10]. We primarily compare our method with self-supervised counterparts, including SimpleOcc [8], OccNeRF [42], SelfOcc [10], DistillNeRF [31], GaussianOcc [7], GaussianTR [13], VEON [45], and LangOcc [2]. These methods represent a broad range of self-supervised occupancy research and include both NeRF [22]

| Method | 3D GT | Pretraining | FPS | mIoU \uparrow | barr | bike | bus | car | e-veh | moto | ped | t-cone | trail | truck | d-surf | s-walk | terr | mann | vege |
|--|--------|----------------|-----|-----------------|--------------|--------------|--------------|--------------|-------------|--------------|--------------|-------------|-------------|--------------|--------------|--------------|--------------|--------------|--------------|
| BEVFormer _(ECCV'22) [19] | Dense | \sim 250 hrs | 3.0 | 26.88 | 37.83 | 17.87 | 40.44 | 42.43 | 7.36 | 23.88 | 21.81 | 20.98 | 22.38 | 30.70 | 55.35 | 36.0 | 28.06 | 20.04 | 17.69 |
| CTF-Occ _(NeurIPS'23) [28] | | \sim 175 hrs | 2.6 | 28.53 | 39.33 | 20.56 | 38.29 | 42.24 | 16.93 | 24.52 | 22.72 | 21.05 | 22.98 | 31.11 | 53.33 | 37.98 | 33.23 | 20.79 | 18.0 |
| RenderOcc _(ICRA'24) [23] | Sparse | \sim 180 hrs | - | 23.93 | 27.56 | 14.36 | 19.91 | 20.56 | 11.96 | 12.42 | 12.14 | 14.34 | 20.81 | 18.94 | 68.85 | 42.01 | 43.94 | 17.36 | 22.61 |
| OccFlowNet _(WACV'25) [3] | | - | - | 26.14 | 27.50 | 26.00 | 34.00 | 32.00 | 20.40 | 25.90 | 18.60 | 20.20 | 26.00 | 28.70 | 62.00 | 37.80 | 39.50 | 29.00 | 26.80 |
| SimpleOcc _(TTV'24) [8] | | 80 hrs | 9.7 | 7.99 | 0.67 | 1.18 | 3.21 | 7.63 | 1.02 | 0.26 | 1.80 | 0.26 | 1.07 | 2.81 | 40.44 | 18.30 | 17.01 | 13.42 | 10.84 |
| OccNeRF _(ICCV'23) [42] | | 216 hrs | 1.0 | 10.81 | 0.83 | 0.82 | 5.13 | 12.49 | 3.50 | 0.23 | 3.10 | 1.84 | 0.52 | 3.90 | 52.62 | 20.81 | 24.75 | 18.45 | 13.19 |
| SelfOcc _(CVPR'24) [10] | | 384 hrs | 1.1 | 9.30 | 0.15 | 0.66 | 5.46 | 12.54 | 0.00 | 0.80 | 2.10 | 0.00 | 0.00 | 8.25 | 55.49 | 26.30 | 26.54 | 14.22 | 5.60 |
| DistillNeRF _(NeurIPS'24) [31] | x | 768 hrs | 1.0 | 8.93 | 1.35 | 2.08 | 10.21 | 10.09 | 2.56 | 1.98 | 5.54 | 4.62 | 1.43 | 7.90 | 43.02 | 16.86 | 15.02 | 14.06 | 15.06 |
| GaussianOcc _(Arxiv'24) [7] | | 168 hrs | - | 11.26 | 1.79 | 5.82 | 14.58 | 13.55 | 1.30 | 2.82 | 7.95 | 9.76 | 0.56 | 9.61 | 44.59 | 20.10 | 17.58 | 8.61 | 10.29 |
| GaussianTR _(CVPR'25) [13] | | 96 hrs | - | 11.70 | 2.09 | 5.22 | 14.07 | 20.43 | 5.70 | 7.08 | 5.12 | 3.93 | 0.92 | 13.36 | 39.44 | 15.68 | 22.89 | 21.17 | 21.87 |
| VEON _(ECCV'24) [45] | | \sim 350 hrs | 2.0 | 15.14 | 10.40 | 6.20 | 17.70 | 12.70 | 8.50 | 7.60 | 6.50 | 5.50 | 8.20 | 11.80 | 54.50 | 25.50 | 30.20 | 25.40 | 25.40 |
| LangOcc _(3DV'25) [2] | | \sim 70 hrs | 2.0 | 11.84 | 3.10 | 9.00 | 6.30 | 14.20 | 0.40 | 10.80 | 6.20 | 9.00 | 3.80 | 10.70 | 43.70 | 9.50 | 26.40 | 19.60 | 26.40 |
| TT-GaussOcc | x | x | 2.7 | 22.07 | 0.08 | 14.94 | 17.89 | 23.21 | 4.66 | 18.55 | 15.64 | 7.07 | 0.00 | 20.16 | 51.41 | 30.43 | 35.81 | 42.24 | 48.93 |

Table 1. 3D occupancy prediction performance on the **Occ3D-nuScenes** dataset [28]. “Dense” refers to voxel-level 3D annotations, whereas “Sparse” consists of point-level ground truth, both requiring manual efforts. The best results among self-supervised methods are highlighted in bold. Offline pre-training time is reported in GPU hours, calculated by multiplying the number of GPUs by the duration.

| Method | 3D GT | IoU \uparrow | mIoU \uparrow | FPS \uparrow | VRAM \downarrow | barr | bike | bus | car | e-veh | moto | ped | t-cone | trail | truck | d-surf | s-walk | terr | mann | vege |
|--|-------|----------------|-----------------|--------------------|---------------------|-------|-------------|--------------|--------------|-------------|--------------|-------------|-------------|-------|--------------|--------------|-------------|--------------|--------------|--------------|
| C-CO _{Net} [†] _(ICCV'23) [33] | Dense | 20.80 | 13.40 | - | \sim 63 GB | 14.30 | 9.10 | 16.50 | 18.30 | 7.40 | 12.30 | 11.10 | 9.40 | 5.80 | 13.20 | 32.50 | - | - | - | 19.90 |
| SelfOcc [†] _(CVPR'24) [10] | x | 2.09 | 5.02 | 0.9 _{0.2} | 9GB _{12.5} | 0.41 | 0.54 | 2.79 | 7.12 | 0.00 | 0.81 | 1.67 | 0.00 | 0.00 | 5.50 | 2.41 | 3.88 | 3.55 | 1.96 | 2.72 |
| TT-GaussOcc | x | 17.64 | 8.53 | 2.6 _{0.1} | 4GB _{0.5} | 0.03 | 7.12 | 11.31 | 10.95 | 1.85 | 11.41 | 5.73 | 4.01 | 0.00 | 11.62 | 12.49 | 8.23 | 10.83 | 13.29 | 19.03 |

Table 2. 3D occupancy prediction performance on the **nuCraft** dataset [49], which has a finer resolution and broader range. As no prior self-supervised methods have been trained or evaluated at this setting, we modify SelfOcc [10] using its official code as our baseline.

and 3DGS [15] representation. For reference, we also include results from self-supervised methods, serving as upper bounds for performance comparison. Implementation details are provided in the supplementary material.

4.2. Main Results

Results on Occ3D-nuScenes. The experiment results on Occ3D-nuScenes [28] benchmark are shown in Table 1. It is evident that TT-GaussOcc not only eliminates the need for costly offline training but also surpasses the second-best self-supervised method (VEON [45] in the 11th row) with a remarkable 46% mIoU improvement. Notably, TT-GaussOcc even achieves an mIoU comparable to models trained with sparse 3D ground truth. In addition, while both our method and SelfOcc [10] utilize the same VLM (OpenSeeD [43]) for semantic predictions, our approach achieves higher IoU not only for large-area categories such as “manmade” and “vegetation” but also exhibits substantial improvements for smaller objects like “cars” and “pedestrians”. It is important to note that OpenSeeD is not aligned with the labels of nuScenes [4], which prevents it from recognizing the “barrier” and “trailer” categories defined in nuScenes. As a result, both TT-GaussOcc and SelfOcc achieve an IoU close to zero for these two classes. However,

TT-GaussOcc still achieves the best overall performance, highlighting its clear advantages. Integrating with more advanced VLMs could further enhance the performance.

Results on nuCraft. The results on the high-resolution nuCraft [49] dataset are presented in Table 2. Since no prior self-supervised methods have been trained or evaluated in this setting, we adapt SelfOcc [10] from its official implementation as a baseline for comparison. As shown in the table, TT-GaussOcc consistently and significantly outperforms SelfOcc using the same VLM model, demonstrating superior adaptability and robustness across different resolutions. Notably, the perception space in nuCraft is defined by a voxel grid of $512 \times 512 \times 40$, totaling over 10 million voxels. Methods like SelfOcc, which directly predict dense voxel labels, inevitably suffer from increased memory overhead and longer inference times as resolution increases. Table 2 reports the inference FPS and GPU memory consumption of both SelfOcc and TT-GaussOcc on nuCraft, with the differences from Occ3D-nuScenes provided in subscript for reference. The results clearly indicate that as resolution increases, SelfOcc’s memory demand and inference time increase notably, whereas TT-GaussOcc experiences only a mild increase since it predicts only sparse occupancy labels.

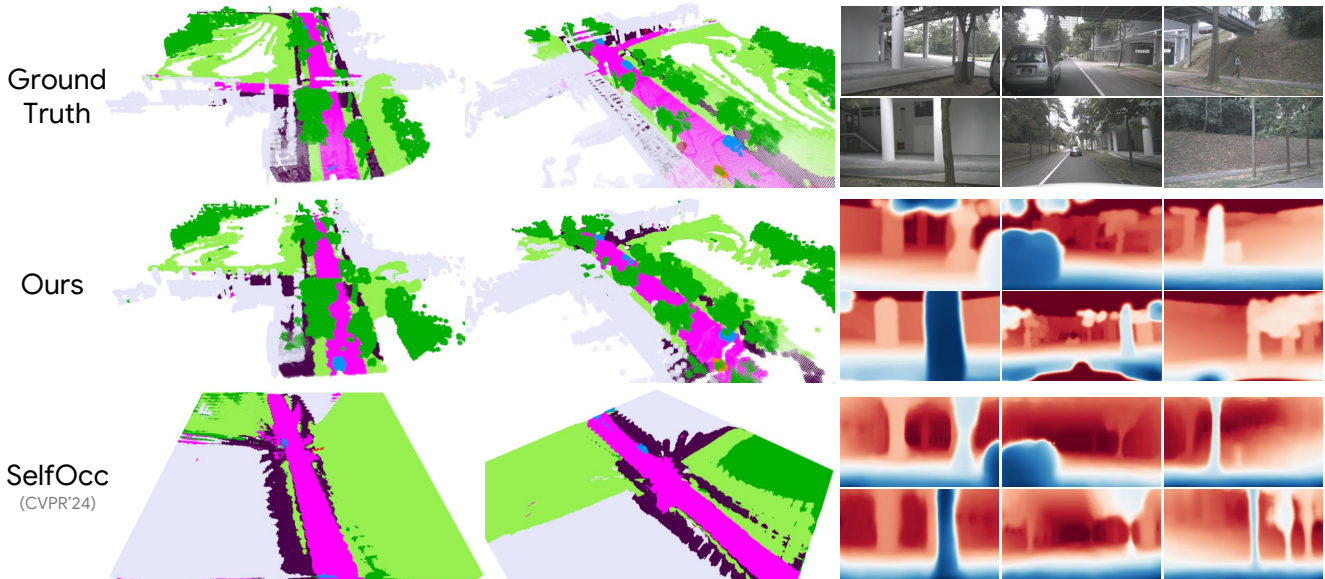


Figure 4. **Qualitative Comparison of 3D Occupancy Prediction.** We compare our method against SelfOcc [10] and the ground truth. The right column shows the corresponding surround-view RGB inputs and generated depth maps. Our approach more accurately reconstructs scene geometry, preserving finer details and capturing object structures with higher fidelity. More visualizations can be found in the supplementary material.

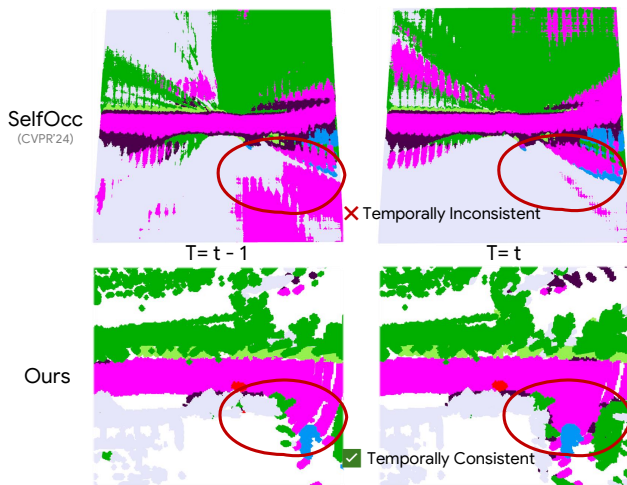


Figure 5. Temporal consistency comparison. We compare the occupancy results of SelfOcc [10] and our method across consecutive frames. The red circles highlight temporal inconsistencies in SelfOcc, in contrast, our method maintains better temporal coherence, effectively preserving scene structures over time.

Qualitative Studies on Temporal Consistency. We present a comprehensive qualitative comparison between TT-GaussOcc and SelfOcc [10] in terms of occupancy prediction and depth rendering in Fig. 4 and temporal consistency in Fig. 5 to demonstrate the semantic and geometry modeling capability. As shown in the figure, SelfOcc exhibits a significant discrepancy from the ground truth, producing noticeably incomplete occupancy predictions. In

contrast, TT-GaussOcc demonstrates a remarkable alignment with the ground truth, accurately recovering intricate structures and preserving high-frequency details in the occupancy representation. Moreover, our rendered depth maps retain fine-grained geometric structures across most regions, further highlighting the effectiveness of our approach in modeling precise scene geometry. These results underscore the superior expressiveness of TT-GaussOcc in both semantic and geometry modeling, showcasing its ability to generate highly realistic and structurally faithful reconstructions.

Case Studies on Open-vocabulary Tasks. TT-GaussOcc inherently supports test-time adaptation to new semantic classes. Since our method directly takes the semantic segmentation results from VLM as input without requiring network pretraining, it fully inherits the open-vocabulary capability of the VLM, enabling open-vocabulary occupancy prediction. Specifically, whenever a new semantic class is detected in the VLM’s output, our method can immediately incorporate it into the occupancy map without any additional training or fine-tuning. Moreover, during Spatiotemporal Smoothing process, Gaussians carrying the newly introduced semantics interact with their neighboring Gaussians, even those that do not originally contain the new class information. This interaction facilitates the propagation of novel semantic categories across the scene, ensuring a more coherent and semantically enriched occupancy representation. As a result, TT-GaussOcc not only captures newly emerging classes in real time but also effectively integrates them into a globally consistent 3D occupancy map.

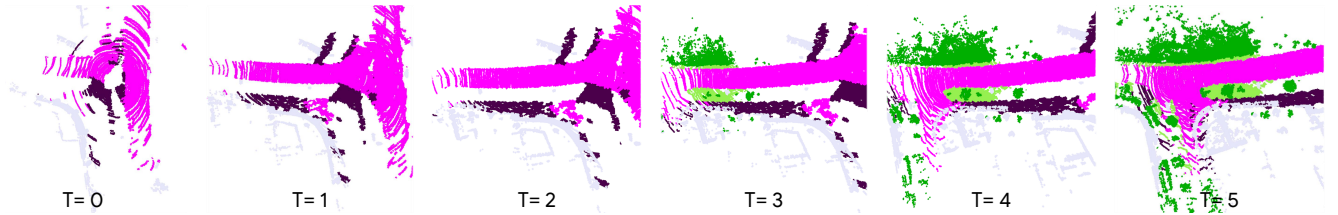


Figure 6. **Progressive Occupancy Estimation in Open-Vocabulary Settings.** We visualize the iterative refinement of TT-GaussOcc over six time steps in an open-vocabulary setting, where the new class query of “vegetation” and “terrain” starts from $T = 3$. This demonstrates the capability of test-time Gaussian optimization to generalize beyond predefined object categories.

| No. | Variant | IoU \uparrow | mIoU \uparrow |
|-------------|--------------------------------|----------------|-----------------|
| A | 3DGS Baseline [15] | 33.5 | 15.1 |
| B | A + Scaling-aware Voxelization | 51.6 | 18.6 |
| C | B + Sigmoid Scale Constraint | 57.2 | 23.7 |
| D | C + Gaussian Flow Estimation | 57.8 | 24.2 |
| TT-GaussOcc | D + TRBF Gaussian Smoothing | 58.1 | 24.9 |

Table 3. Ablation studies of the proposed components.

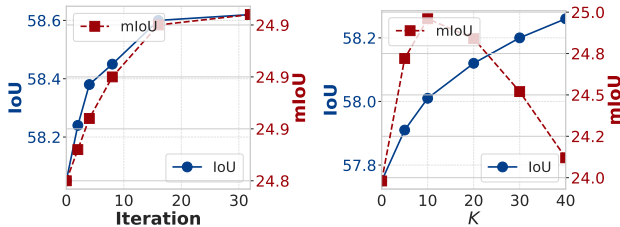


Figure 7. The parameter sensitivity study on the number of optimization iterations and K nearest neighbors on Occ3D-nuScenes.

4.3. Ablation Studies

Impact of Components. To validate the effectiveness of each core component in TT-GaussOcc, we conduct ablation studies on a subset of Occ3D-nuScenes [28]. Specifically, we adopt 3DGS [15] as our baseline, denoted by variant A, which follows the same initialization and optimization procedure as 3DGS and converts Gaussians to voxels by scattering Gaussian centers. As shown in Table 3, this naïve approach yields suboptimal results, highlighting the importance of incorporating additional geometric cues. We then introduce scale-aware Gaussian voxelization using Eq. (10), denoted by variant B. This leads to a substantial performance improvement, demonstrating the necessity of accounting for Gaussian extent during voxelization. Further constraining the scale with a sigmoid activation avoid the excessive growth of Gaussians (variant C), which is an essential problem when points are sparse, yielding additional gains. Finally, integrating temporal Gaussian flow (variant D) and TRBF Gaussian smoothing (TT-GaussOcc) further enhances the results by leveraging motion cues and multi-frame consistency, respectively. The consistent performance improvements across all stages underscore the ef-

fectiveness of our design choices in achieving robust and high-fidelity occupancy predictions.

Parameter Sensitivity. We further investigate the impact of two key factors on occupancy prediction performance. First, we analyze the effect of the neighborhood size K in spatiotemporal smoothing. As K increases from 0 (*i.e.*, no fusion) to 10, both IoU and mIoU improve, indicating the effectiveness of fusion in enhancing spatial consistency. However, beyond $K = 10$, while IoU continues to increase, mIoU starts to decline, suggesting that excessive fusion may introduce over-smoothing effects. Considering both performance and computational efficiency, we set $K = 10$ as the optimal choice. Second, we examine the relationship between training iterations and performance. The results show that within a moderate range, IoU and mIoU exhibit an approximately linear increase with more iterations, but the overall improvement remains limited. This suggests that beyond a certain point, additional training yields diminishing returns. Therefore, we recommend adjusting the number of iterations to balance accuracy and efficiency based on specific application requirements.

5. Conclusion

In this work, we introduce TT-GaussOcc, an efficient and reliable method for occupancy prediction that removes the requirement for expensive pre-training and supports dynamic, real-time adaptation to varying object classes and spatial resolutions. Extensive experiments conducted on Occ3D-nuScenes and nuCraft demonstrate both quantitatively and qualitatively that TT-GaussOcc effectively scales to higher resolutions, achieving up to a 45% improvement in mIoU. Nevertheless, sparse initialization of Gaussians can cause inaccuracies in Gaussian flows and lifted semantics, which are difficult to correct without explicit 3D supervision. Although trilateral smoothing partially mitigates this issue, accumulating point clouds across multiple sweeps could further densify Gaussians and improve reconstruction quality at the expense of higher inference-time costs. Future work will explore methods to balance reconstruction accuracy and computational efficiency.

References

- [1] Shariq Farooq Bhat, Reiner Birkel, Diana Wofk, Peter Wonka, and Matthias Müller. Zoedepth: Zero-shot transfer by combining relative and metric depth. *CoRR*, abs/2302.12288, 2023. 2
- [2] Simon Boeder, Fabian Gigengack, and Benjamin Risse. Langocc: Self-supervised open vocabulary occupancy estimation via volume rendering. *arXiv preprint arXiv:2407.17310*, 2024. 2, 5, 6
- [3] Simon Boeder, Fabian Gigengack, and Benjamin Risse. Occlownet: Towards self-supervised occupancy estimation via differentiable rendering and occupancy flow. *arXiv preprint arXiv:2402.12792*, 2024. 2, 6
- [4] Holger Caesar, Varun Bankiti, Alex H. Lang, Sourabh Vora, Venice Erin Liong, Qiang Xu, Anush Krishnan, Yu Pan, Giancarlo Baldan, and Oscar Beijbom. nuscenes: A multimodal dataset for autonomous driving. In *CVPR*, pages 11618–11628, 2020. 5, 6
- [5] Ricardo J. G. B. Campello, Davoud Moulavi, and Joerg Sander. Density-based clustering based on hierarchical density estimates. In *Advances in Knowledge Discovery and Data Mining*, pages 160–172, 2013. 4
- [6] Ziyu Chen, Jiawei Yang, Jiahui Huang, Riccardo de Lutio, Janick Martinez Esturo, Boris Ivanovic, Or Litany, Zan Gojic, Sanja Fidler, Marco Pavone, Li Song, and Yue Wang. Omnire: Omni urban scene reconstruction. In *ICLR*, 2025. 2, 3
- [7] Wanshui Gan, Fang Liu, Hongbin Xu, Ningkai Mo, and Naoto Yokoya. Gaussianocc: Fully self-supervised and efficient 3d occupancy estimation with gaussian splatting. *arXiv preprint arXiv:2408.11447*, 2024. 2, 5, 6
- [8] Wanshui Gan, Ningkai Mo, Hongbin Xu, and Naoto Yokoya. A comprehensive framework for 3d occupancy estimation in autonomous driving. *IEEE TIV*, pages 1–19, 2024. 2, 5, 6
- [9] Yuanhui Huang, Wenzhao Zheng, Yunpeng Zhang, Jie Zhou, and Jiwen Lu. Tri-perspective view for vision-based 3d semantic occupancy prediction. In *CVPR*, pages 9223–9232, 2023. 2
- [10] Yuanhui Huang, Wenzhao Zheng, Borui Zhang, Jie Zhou, and Jiwen Lu. Selfocc: Self-supervised vision-based 3d occupancy prediction. In *CVPR*, pages 19946–19956, 2024. 2, 4, 5, 6, 7
- [11] Yuanhui Huang, Wenzhao Zheng, Yunpeng Zhang, Jie Zhou, and Jiwen Lu. Gaussianformer: Scene as gaussians for vision-based 3d semantic occupancy prediction. In *ECCV*, pages 376–393, 2024. 2
- [12] Haoyi Jiang, Tianheng Cheng, Naiyu Gao, Haoyang Zhang, Tianwei Lin, Wenyu Liu, and Xinggang Wang. Symphonize 3d semantic scene completion with contextual instance queries. In *IEEE/CVF Conference on Computer Vision and Pattern Recognition, CVPR 2024, Seattle, WA, USA, June 16-22, 2024*, pages 20258–20267. IEEE, 2024. 2
- [13] Haoyi Jiang, Liu Liu, Tianheng Cheng, Xinjie Wang, Tianwei Lin, Zhizhong Su, Wenyu Liu, and Xinggang Wang. Gausstr: Foundation model-aligned gaussian transformer for self-supervised 3d spatial understanding. *arXiv preprint arXiv:2412.13193*, 2024. 2, 5, 6
- [14] Kapil D. Katyal, Adam Polevoy, Joseph Moore, Craig Knuth, and Katie M. Popek. High-speed robot navigation using predicted occupancy maps. In *ICRA*, pages 5476–5482, 2021. 2
- [15] Bernhard Kerbl, Georgios Kopanas, Thomas Leimkuehler, and George Drettakis. 3d gaussian splatting for real-time radiance field rendering. *ACM TOG*, 42(4), 2023. 2, 4, 6, 8
- [16] Seungjae Lee, Hyungtae Lim, and Hyun Myung. Patchwork++: Fast and robust ground segmentation solving partial under-segmentation using 3d point cloud. In *IROS*, pages 13276–13283, 2022. 4
- [17] Bohan Li, Jiajun Deng, Wenyao Zhang, Zhujin Liang, Dalong Du, Xin Jin, and Wenjun Zeng. Hierarchical temporal context learning for camera-based semantic scene completion. In *Computer Vision - ECCV 2024 - 18th European Conference, Milan, Italy, September 29-October 4, 2024, Proceedings, Part IV*, pages 131–148. Springer, 2024. 2
- [18] Yiming Li, Zhiding Yu, Christopher B. Choy, Chaowei Xiao, José M. Álvarez, Sanja Fidler, Chen Feng, and Anima Anandkumar. Voxformer: Sparse voxel transformer for camera-based 3d semantic scene completion. In *IEEE/CVF Conference on Computer Vision and Pattern Recognition, CVPR 2023, Vancouver, BC, Canada, June 17-24, 2023*, pages 9087–9098. IEEE, 2023. 2
- [19] Zhiqi Li, Wenhai Wang, Hongyang Li, Enze Xie, Chonghao Sima, Tong Lu, Yu Qiao, and Jifeng Dai. Bevformer: Learning bird’s-eye-view representation from multi-camera images via spatiotemporal transformers. In *ECCV*, pages 1–18, 2022. 6
- [20] Yancong Lin and Holger Caesar. Icp-flow: Lidar scene flow estimation with icp. In *CVPR*, pages 15501–15511, 2024. 4
- [21] Yuhang Lu, Xinge Zhu, Tai Wang, and Yuexin Ma. Octreeocc: Efficient and multi-granularity occupancy prediction using octree queries. *CoRR*, abs/2312.03774, 2023. 2
- [22] Ben Mildenhall, Pratul P. Srinivasan, Matthew Tancik, Jonathan T. Barron, Ravi Ramamoorthi, and Ren Ng. NeRF: Representing scenes as neural radiance fields for view synthesis. In *ECCV*, pages 405–421, 2020. 5
- [23] Mingjie Pan, Jiaming Liu, Renrui Zhang, Peixiang Huang, Xiaoqi Li, Hongwei Xie, Bing Wang, Li Liu, and Shanghang Zhang. Renderocc: Vision-centric 3d occupancy prediction with 2d rendering supervision. In *ICRA*, pages 12404–12411, 2024. 2, 6
- [24] Alec Radford, Jong Wook Kim, Chris Hallacy, Aditya Ramesh, Gabriel Goh, Sandhini Agarwal, Girish Sastry, Amanda Askell, Pamela Mishkin, Jack Clark, Gretchen Krueger, and Ilya Sutskever. Learning transferable visual models from natural language supervision. In *Proceedings of the 38th International Conference on Machine Learning, ICML 2021, 18-24 July 2021, Virtual Event*, pages 8748–8763. PMLR, 2021. 2
- [25] René Ranftl, Katrin Lasinger, David Hafner, Konrad Schindler, and Vladlen Koltun. Towards robust monocular depth estimation: Mixing datasets for zero-shot cross-dataset transfer. *IEEE Trans. Pattern Anal. Mach. Intell.*, 44(3):1623–1637, 2022. 2

- [26] Sebastian Raschka, Joshua Patterson, and Corey Nolet. Machine learning in python: Main developments and technology trends in data science, machine learning, and artificial intelligence. *arXiv preprint arXiv:2002.04803*, 2020. 4
- [27] Pin Tang, Zhongdao Wang, Guoqing Wang, Jilai Zheng, Xiangxuan Ren, Bailan Feng, and Chao Ma. Sparseocc: Rethinking sparse latent representation for vision-based semantic occupancy prediction. In *IEEE/CVF Conference on Computer Vision and Pattern Recognition, CVPR 2024, Seattle, WA, USA, June 16-22, 2024*, pages 15035–15044. IEEE, 2024. 2
- [28] Xiaoyu Tian, Tao Jiang, Longfei Yun, Yucheng Mao, Huitong Yang, Yue Wang, Yilun Wang, and Hang Zhao. Occ3d: a large-scale 3d occupancy prediction benchmark for autonomous driving. In *NeurIPS*, 2023. 2, 5, 6, 8
- [29] Antonín Vobecký, Oriane Siméoni, David Hurych, Spyridon Gidaris, Andrei Bursuc, Patrick Pérez, and Josef Sivic. POP-3D: open-vocabulary 3d occupancy prediction from images. In *Advances in Neural Information Processing Systems 36: Annual Conference on Neural Information Processing Systems 2023, NeurIPS 2023, New Orleans, LA, USA, December 10 - 16, 2023*, 2023. 2
- [30] Lizi Wang, Hongkai Ye, Qianhao Wang, Yuman Gao, Chao Xu, and Fei Gao. Learning-based 3d occupancy prediction for autonomous navigation in occluded environments. In *IROS*, pages 4509–4516, 2021. 2
- [31] Letian Wang, Seung Wook Kim, Jiawei Yang, Cunjun Yu, Boris Ivanovic, Steven Waslander, Yue Wang, Sanja Fidler, Marco Pavone, and Peter Karkus. Distillnerf: Perceiving 3d scenes from single-glance images by distilling neural fields and foundation model features. In *NeurIPS*, pages 62334–62361, 2024. 2, 4, 5, 6
- [32] Lening Wang, Wenzhao Zheng, Yilong Ren, Han Jiang, Zhiyong Cui, Haiyang Yu, and Jiwen Lu. Occsora: 4d occupancy generation models as world simulators for autonomous driving, 2024. 3
- [33] Xiaofeng Wang, Zheng Zhu, Wenbo Xu, Yunpeng Zhang, Yi Wei, Xu Chi, Yun Ye, Dalong Du, Jiwen Lu, and Xingang Wang. Openoccupancy: A large scale benchmark for surrounding semantic occupancy perception. In *2023 IEEE/CVF International Conference on Computer Vision (ICCV)*, pages 17804–17813, 2023. 6
- [34] Yuqi Wang, Yuntao Chen, Xingyu Liao, Lue Fan, and Zhaoxiang Zhang. Panoocc: Unified occupancy representation for camera-based 3d panoptic segmentation. In *IEEE/CVF Conference on Computer Vision and Pattern Recognition, CVPR 2024, Seattle, WA, USA, June 16-22, 2024*, pages 17158–17168. IEEE, 2024. 2
- [35] Yi Wei, Linqing Zhao, Wenzhao Zheng, Zheng Zhu, Jie Zhou, and Jiwen Lu. Surroundocc: Multi-camera 3d occupancy prediction for autonomous driving. In *ICCV*, pages 21672–21683, 2023. 2
- [36] Zihao Wen, Yifan Zhang, Xinhong Chen, Jianping Wang, Yung-Hui Li, and Yu-Kai Huang. Tofg: Temporal occupancy flow graph for prediction and planning in autonomous driving. *IEEE TIV*, 9(1):2850–2863, 2024. 2
- [37] Siyuan Wu, Gang Chen, Moji Shi, and Javier Alonso-Mora. Decentralized multi-agent trajectory planning in dynamic environments with spatiotemporal occupancy grid maps. In *ICRA*, pages 7208–7214, 2024. 2
- [38] Yunzhi Yan, Haotong Lin, Chenxu Zhou, Weijie Wang, Haiyang Sun, Kun Zhan, Xianpeng Lang, Xiaowei Zhou, and Sida Peng. Street gaussians for modeling dynamic urban scenes. *CoRR*, abs/2401.01339, 2024. 3
- [39] Jiawei Yang, Boris Ivanovic, Or Litany, Xinshuo Weng, Seung Wook Kim, Boyi Li, Tong Che, Danfei Xu, Sanja Fidler, Marco Pavone, et al. Emernerf: Emergent spatial-temporal scene decomposition via self-supervision. In *ICLR*, 2024. 2
- [40] Ze Yang, Yun Chen, Jingkang Wang, Sivabalan Manivasagam, Wei-Chiu Ma, Anqi Joyce Yang, and Raquel Urtasun. Unisim: A neural closed-loop sensor simulator. In *2023 IEEE/CVF Conference on Computer Vision and Pattern Recognition (CVPR)*, pages 1389–1399, 2023. 2
- [41] Chi Zhang, Shirui Ma, Muzhi Wang, Gereon Hinz, and Alois Knoll. Efficient pomdp behavior planning for autonomous driving in dense urban environments using multi-step occupancy grid maps. In *ITSC*, pages 2722–2729, 2022. 2
- [42] Chubin Zhang, Juncheng Yan, Yi Wei, Jiaxin Li, Li Liu, Yansong Tang, Yueqi Duan, and Jiwen Lu. Occnerf: Advancing 3d occupancy prediction in lidar-free environments. *arXiv preprint arXiv:2312.09243*, 2023. 2, 5, 6
- [43] Hao Zhang, Feng Li, Xueyan Zou, Shilong Liu, Chunyuan Li, Jianwei Yang, and Lei Zhang. A simple framework for open-vocabulary segmentation and detection. In *ICCV*, pages 1020–1031, 2023. 4, 6
- [44] Yunpeng Zhang, Zheng Zhu, and Dalong Du. Occformer: Dual-path transformer for vision-based 3d semantic occupancy prediction. In *ICCV*, pages 9399–9409, 2023. 2
- [45] Jilai Zheng, Pin Tang, Zhongdao Wang, Guoqing Wang, Xiangxuan Ren, Bailan Feng, and Chao Ma. Veon: Vocabulary-enhanced occupancy prediction. In *ECCV*, pages 92–108, 2024. 2, 5, 6
- [46] Wenzhao Zheng, Weiliang Chen, Yuanhui Huang, Borui Zhang, Yueqi Duan, and Jiwen Lu. Occworld: Learning a 3d occupancy world model for autonomous driving. In *ECCV*, pages 55–72, 2024. 3
- [47] Hongyu Zhou, Jiahao Shao, Lu Xu, Dongfeng Bai, Weichao Qiu, Bingbing Liu, Yue Wang, Andreas Geiger, and Yiyi Liao. HUGS: holistic urban 3d scene understanding via gaussian splatting. In *IEEE/CVF Conference on Computer Vision and Pattern Recognition, CVPR 2024, Seattle, WA, USA, June 16-22, 2024*, pages 21336–21345. IEEE, 2024. 3
- [48] Xiaoyu Zhou, Zhiwei Lin, Xiaojun Shan, Yongtao Wang, Deqing Sun, and Ming-Hsuan Yang. Drivinggaussian: Composite gaussian splatting for surrounding dynamic autonomous driving scenes. In *IEEE/CVF Conference on Computer Vision and Pattern Recognition, CVPR 2024, Seattle, WA, USA, June 16-22, 2024*, pages 21634–21643. IEEE, 2024. 2, 3, 4, 5
- [49] Benjin Zhu, Zhe Wang, and Hongsheng Li. nucraft: Crafting high resolution 3d semantic occupancy for unified 3d scene understanding. In *ECCV*, pages 125–141, 2024. 2, 5, 6